Kybernetik 12, 185—203 (1973)

A Theory of the Pattern Induced Flight Orientation of the Fly *Musca Domestica*

T. Poggio and W. Reichardt
Max-Planck-Institut für biologische Kybernetik, Tübingen, FRG

Received: December 8, 1972

Abstract

The theory presented here describes the visual orientation behavior of fixed flying insects (the fly *Musca domestica*) in the presence of elementary patterns. The theory, which is based on a number of experimental results, Reichardt (1973), is a phenomenological one whose main purpose is to provide an organizational framework for treating a complex phenomenon without the need of detailed assumptions about the neural mechanisms actually involved.

A simple hypothesis concerning the basic structure of the pattern fixation process leads to an equivalent stochastic equation of the *Langevin* type, which can be linearized for simple single-stripe panoramas. A critical experiment supports these theoretical assumptions. In addition, the effect on pattern fixation behavior of adding contrast noise to the background of the panorama, is quantitatively predicted by the theory.

In the more general case of a panorama consisting of many vertical stripes, the *Fokker-Planck* equation associated with the *Langevin* equation, no longer linear, is solved. Making use of an experimentally proven "superposition principle", the stationary pattern fixation behavior of the fly in an arbitrary panorama consisting of a collection of vertical stripes is predicted. In this context, concepts like pseudo-invariance and phase-transition can be applied to the insects orientation behavior. The theory presented here seems to contain rich classification properties, which might provide the foundations for an understanding of more complex pattern discrimination processes.

Possible extensions of the theory, as well as some similarities to human eye fixation, are also discussed.

1.0. Introduction

Behavioral investigations of visual detection, fixation and discrimination of elementary patterns by fixed flying flies, which have been recently undertaken in our laboratory, have led to quantitative results whose analysis and interpretation has been given by one of us; Reichardt (1973)[1]. The purpose of this paper is to outline a theoretical approach to the analysis of the processes involved in the orientation (fixation) of the fly towards elementary patterns in the presence and absence of contrast noise.

As a first step we correlate the analysis neither with the present knowledge concerning the structure and function of the nervous elements in the optical ganglia or midbrain of the fly nor with the model describing movement perception [see for instance Reichardt (1961)], but rather prefer a phenomenological approach for the interpretation and analysis of the experimental data. In this approach, we shall take into account some of the more basic experimental findings and formulate an equivalent mathematical structure from which we deduce and interpret the behavior of the fly under more complex stimulus conditions.

2.0. Conception and Methods

The experimental set-up which has been used in order to measure the behavior of fixed flying flies under closed-loop conditions (interaction between the fly and its optical surroundings) has already been described, Reichardt (1973), but is presented here again in Fig. 1. Its main components are: a) a flight-torque compensator, b) an analog electronic device which controls the motor speed according to the torque signal generated by the fly, c) a servomotor which drives a patterned cylindrical panorama.

Female, wild-type, red-eyed *Musca domestica* from a laboratory stock were used as test-flies for these investigations.

During the experiments, a test-fly, with head fixed to the thorax is suspended from the compensator on the axis of the cylindrical panorama. The panorama, which carries on its inner surface the individual test patterns, is homogeneously illuminated with a brightness, standard for all the experiments described here, of about 5500 Apostilb (1 Apostilb = 10^{-4} Lambert).

For a fly suspended from the compensator, the six degrees of freedom (three for translations and three for rotations) are blocked. However the coupling of the visual environment to the output of the torque compensator simulates one degree of freedom, namely the rotation around the fly's vertical axis in horizontal flight. The equivalent behavior of a fly under free flight conditions would be a rotation around its vertical axis with respect to an optical environment positioned sufficiently distant to the fly so that the translational flight components do not contribute to displacements of the imaged surroundings on the retinae of the two compound eyes.

The electronic analog device connecting the compensator output, whose voltage is proportional to the instantaneous torque signal generated by the fly, to the servomotor system, simulates the

[1] Preliminary results have been published in the following papers: Reichardt and Wenking (1969); Reichardt (1969a), (1970), (1971a), (1971b).

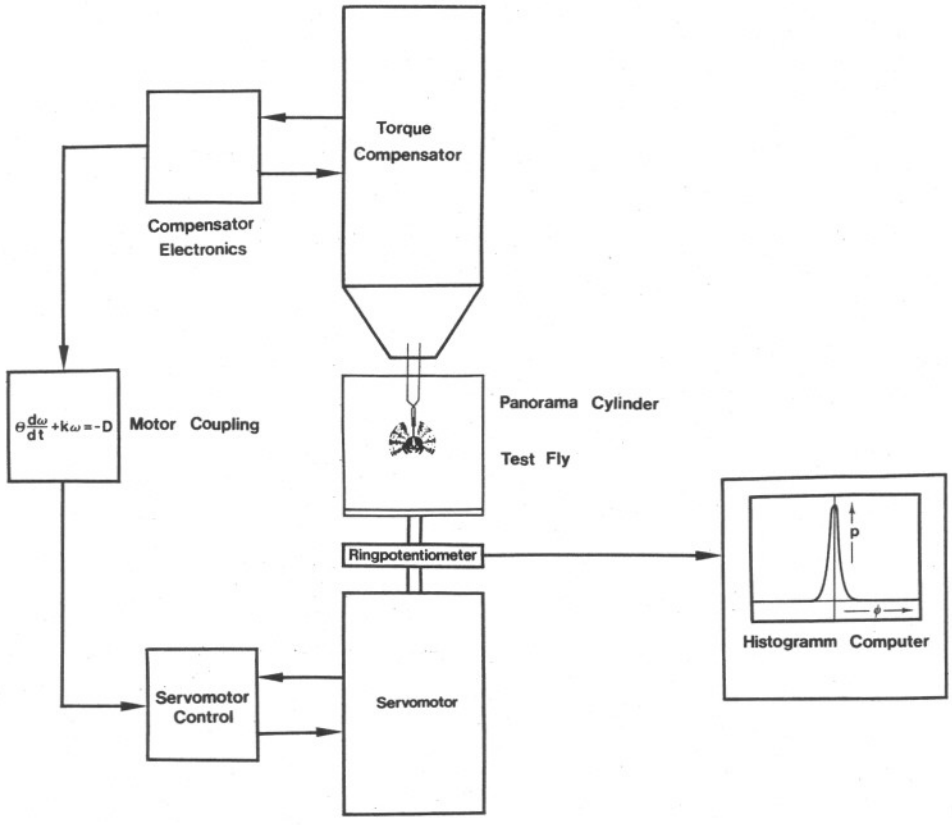

Fig. 1. Simplified diagram of the experimental set-up (closed loop system). A test fly, suspended from the torque compensator, is enabled to control the position of a patterned panorama by its own torque signal. The transfer conditions of the compensator, the motor coupling block and the servomotor give an approximation of the dynamics of the equivalent free-flight conditions. The instantaneous position of the panorama is signaled from a ring potentiometer and evaluated by a computer. For more details, see the text

free flight dynamics or, more exactly, a simple approximation of it expressed by the equation

$$\Theta\ddot{\psi}+k\dot{\psi}=-D(t)\,, \tag{1}$$

where ψ is the angular position of the cylindrical panorama, $\dot{\psi}$ and $\ddot{\psi}$ represent the first and second time derivatives, Θ is the moment of inertia of the fly around its vertical axis {measured as about 1.5×10^{-3} [gr · cm^2]} and k the friction experienced by the fly under rotation around its vertical axis in free flight. The exact value of k for free flight conditions is not yet known. In our experiments k is therefore treated as a parameter ranging from 0.375 to 0.028 [gr · cm^2 sec^{-1}]. Equation (1) defines the "coupling" of the fly to the panorama, which depends upon the parameters Θ and k. Different degrees of coupling, which result in different asymptotic values of the panorama speed for a given constant value of the torque D, can be expressed, since Θ is a constant, by the single parameter $\frac{\Theta}{k}$ [sec]. The speed is in fact proportional to this value: for example, a constant torque signal of 1 [dyne · cm] results in an asymptotic angular speed of 152.7 [degrees · sec^{-1}] when $\frac{\Theta}{k}=4\cdot10^{-3}$ [sec].

The details of the torque compensator have already been described, Fermi and Reichardt (1963); Götz (1964). The input (torque) – output (voltage) transfer response of the compensator, expressed as its amplitude-frequency and phase-frequency characteristics, is flat over the low frequency range. The relative amplitude decreases by -3 db at a frequency of about 60 Hz. The frequency spectrum of the torque signal generated by a fly, measured in closed loop from the compensator output, contains its significant power in the frequency range from zero to 10 Hz. Since the compensator transfer response is flat up to 10 Hz and exhibits a maximum phase angle of only 5° at this frequency, it is logical to conclude that the output of the torque-compensator is proportional to the torque signal generated by a fixed flying test-fly.

The electronic analog device has the following transfer function, corresponding to Eq. (1)

$$L(i2\pi f)=\frac{1}{\Theta}\cdot\frac{1}{i2\pi f+\frac{k}{\Theta}}\,, \tag{2}$$

where f is the frequency.

Since the transfer function of the servomotor drive system (excited by 400 Hz) is flat from zero to about 20 Hz and the input spectrum cannot be wider than the torque spectrum because of the lowpass filter properties of the interconnecting electronic analog device, no signal distortion is introduced by the system. As a consequence, the complete transfer function of the experimental set-up, consisting of the compensator, the analog electronics and the servomotor drive system, reduces to the linear transfer function of Eq. (2); electronic noise and drifts are negligible.

The instantaneous angular position $\psi(t)$ of the pattern is signaled by a ring-potentiometer mounted on the servomotor shaft, which also carries the rotating cylindrical panorama; the resulting displacement signal is sampled by a multichannel analyser (Didac 800, Deutsche Intertechnique) which calculates and plots amplitude histograms of the pattern position. Further methods of analysis and other modes of operation of the device will be described in the text.

A diagram describing the information flow between the fly and its optical surroundings under our experimental conditions is presented in Fig. 2 in the form of a black box scheme. The mechanical-electronic device which couples the fly to its visual surroundings is given by the linear filter L, whose transfer properties are simply expressed in Eq. (2). F indicates the nonlinear, generally time-varying, black box which represents the fixed, flying test-fly. The output of the box L is connected to the input of the box F since the optical surroundings of the fly strongly influence its behavior.

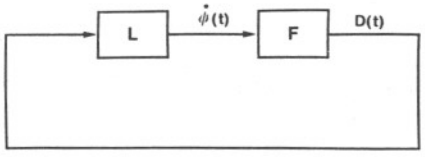

Fig. 2. The overall information flow diagram of the experimental set-up described in Fig. 1. The functional properties of the fly, observed under our experimental conditions, are represented by the black box F. L stands for the transfer properties of the analog electronics which simulates free flight conditions (rotation around the fly's vertical axis). The test fly perceives an angular speed $\dot{\psi}(t)$ of the panorama and generates a torque signal $D(t)$

3.0. Results

In the preceding chapter the transfer function of the box L has been specified. So far we have not given any specification concerning the box F, which describes the behavior of the fly during the experiments. Therefore it appears necessary to summarise here some of the experimental results described by Reichardt (1973) from which we shall derive the key properties for the characterization of F.

3.1. Fixation of a Single Black Stripe

When a test-fly is coupled to the white, homogeneously illuminated panorama which carries a single black, vertically oriented stripe, the panorama is rotated by the fly until the stripe has reached the average position $\psi = 0^0$, about which it oscillates in a random-like motion. This position is characterized by the fly's direction of flight; therefore we may state

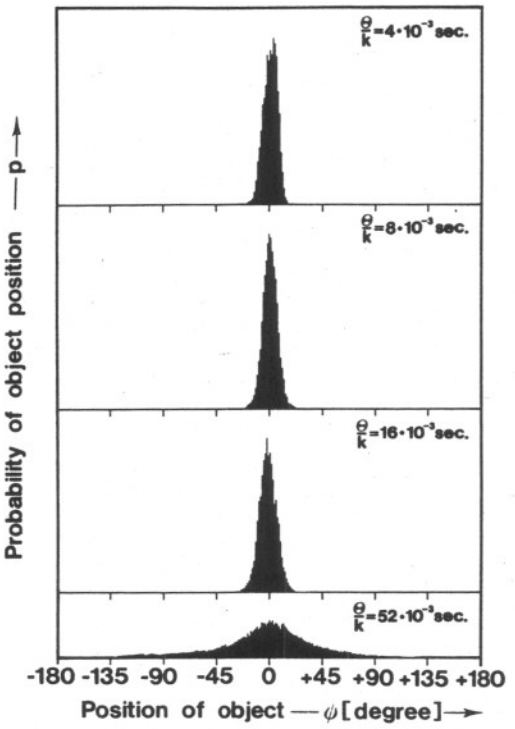

Fig. 3. Position histograms, obtained from a test fly during the stationary phase of fixation of a single, black, vertically oriented stripe of 5° angular width. The parameter of the experiment is the coupling constant $\frac{\Theta}{k}$ [sec]

that the fly is fixating the stripe. Fixation of the stripe takes place irrespective of the panorama's initial position. Fig. 3 shows a sequence of histograms describing fixation for different coupling-in conditions, expressed by the parameter $\frac{\Theta}{k}$. These histograms represent the probability of the stripe's position. As can be easily seen from Fig. 3, the half-width of these histograms increases for increasing coupling. A first possible explanation for this finding is that with increasing coupling the relative velocity of the stripe increases, which must finally lead to a decrease in the fly's ability to perceive its motion.

3.2. Elementary Processes Involved in the Fixation Behavior

In a series of experiments it has been shown by Reichardt (1973) that the fixation behavior rests on two observations and a simple fact. The first observation is that a test-fly generates a symmetric stochastic torque signal $N(t)$ if the panorama is not coupled to the fly

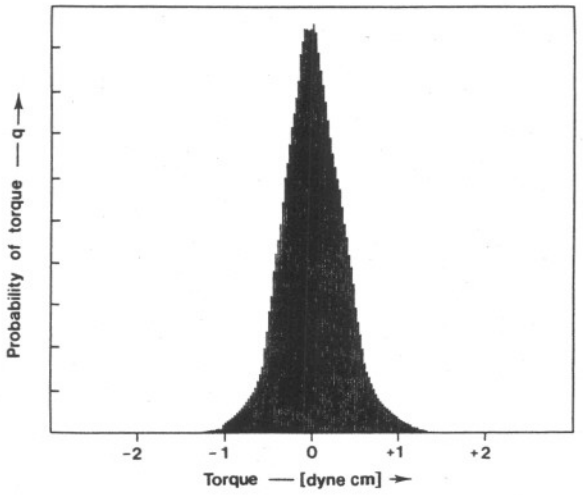

Fig. 4a. Histogram of the torque fluctuation generated by a fly in a contrastless, uniformly illuminated environment (open loop). As shown by a statistical test using the coefficients of "skewness" and "excess", the histogram is a good approximation to a gaussian distribution. The σ^2 of the histogram determines the power of the zero-mean torque fluctuation

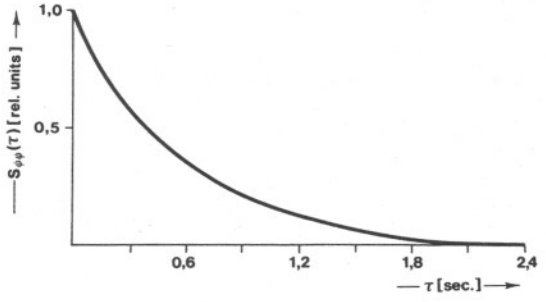

Fig. 4b. Normalized autocorrelation function of the open loop torque fluctuation whose histogram is shown in Fig. 4a. The autocorrelation function is very well approximated by the exponential expression $\frac{S_{\psi,\psi}(\tau)}{S_{\psi,\psi}(0)} = e^{-\gamma|\tau|}$. In this case $\gamma = 1.9\ [\text{sec}^{-1}]$

(open loop condition). A typical example of this process is given in Fig. 4a in the form of a torque histogram, which turns out to be, in very good approximation, gaussian. The corresponding normalized autocorrelation function, shown in Fig. 4b, is approximately given by $e^{-\frac{\tau}{\tau_0}}$. It declines to $\frac{1}{e}$ for $\tau_0 = 0.526$ [sec]; therefore $\frac{1}{\tau_0} = \gamma = 1.9\ [\text{sec}^{-1}]$. The second observation clearly goes beyond the well known findings for the optomotor response described in insects [for a review see Reichardt (1969b)]; namely, the strength of the optomotor response for progressive

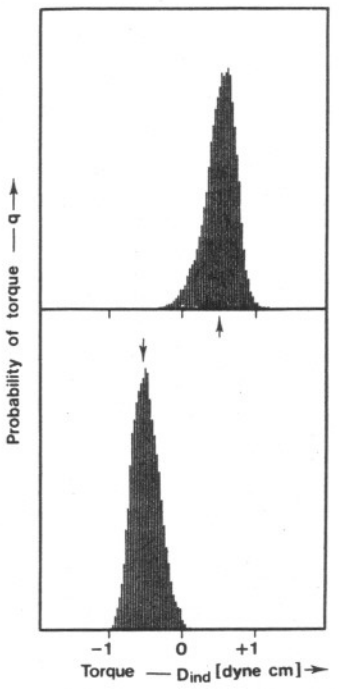

Fig. 5. Histograms of the torque output of a test fly in open loop when a vertical black stripe of 1° angular width is oscillating symmetrically about the angular positions +90° (upper) and −90° (lower). The stripe is driven by a stochastic process with a maximum amplitude of ±5° and a high-frequency cut-off at ~5 Hz. The difference between the mean values of the distributions is highly significant

stripe motion (from the front of one of the compound eyes to the back) is stronger than for regressive stripe motion (from back to front). This is shown in Fig. 5, where we present two torque histograms recorded under open loop conditions with symmetric random stripe-motions about the positions $\psi_0 = \pm 90°$. The centres of gravity of the two histograms are significantly separated, indicating that under these conditions the test-fly tries to approach the moving stripe. We may now state that there is a second type of torque response, a reaction induced by the motion of the pattern; this response is an asymmetric one. The third point is the fact that the fly has two compound eyes with a line of symmetry between the two. Combining these two observations from open loop experiments and taking into consideration the symmetry line, the fixation process observed under closed loop conditions can be easily derived: the random torque signal $N(t)$ elicits a symmetric fluctuation of the stripe which in turn results in an asymmetric induced torque response driving the stripe towards the direction of flight where it is stabilized due to the symmetry between the two eyes.

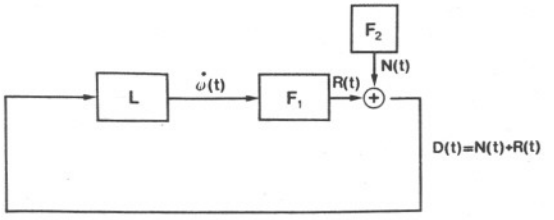

Fig. 6. Equivalent information flow diagram of the dynamical model. The black box F – representing the "fixating fly" – is conceptually separated into two subsystems: F_1, associated with the asymmetric optomotor reaction, and F_2, representing the source of the stochastic torque process. The basic hypothesis implied in the diagram and discussed in the text is that the optomotor signal $R(t)$ and the noise process $N(t)$ are independent and additive

We are now in a position to develop the scheme presented in Fig. 2 into the more detailed one shown in Fig. 6. In this figure the F-box has been split into two parts, F_1 and F_2, according to our knowledge about the stochastic torque signal $N(t)$ and the induced torque response $R(t)$. The assumption is made that $N(t)$ and $R(t)$ are interacting simply by addition. In the next chapter, experimental evidence supporting this assumption will be given.

3.3. General Mathematical Description of the Fixation Process

Reading the dynamical equation of the whole system from the network diagram in Fig. 6 and taking into account Eqs. (1) or (2), we obtain the equation

$$\ddot{\psi}(t)+\frac{k}{\Theta}\dot{\psi}(t)=\frac{1}{\Theta}N(t)-\frac{1}{\Theta}F_1\{\psi(t'),\dot{\psi}(t')\}, \quad (3)$$

where F_1 is a function of the angular position and velocity of a given pattern describing the induced reponse of the fly, which must, in principle, be delayed ($t'=t-\varepsilon$). As has been stated before, $N(t)$, the torque signal generated by the fly, is a zero-mean random process, therefore the sign of $N(t)$ in Eq. (3) is not important. The gaussianity of the recorded histograms (Fig. 4a) suggests the assumption that $N(t)$ is also gaussian.

The assumptions implied by Eq. (3) are the following:

a) N is a stationary random process and F_1 does not depend explicitly on the time t.

b) F_1 is significantly dependent only upon ψ and $\dot{\psi}$.

c) Following experimental evidence to be given in Section 3.4, N does not depend significantly on ψ and $\dot{\psi}$. Therefore we assume that N is characterized by the open loop torque signal.

Equation (3) is an equation of the generalized *Langevin* type, describing the "motion" of our dynamic system.

Interestingly, the form of Eq. (3) leads to a straightforward analogy between the fixation process described here and the quasi-brownian motion of a particle in a potential hole. The equivalent of a potential hole is implied by the experimental fact that the one-dimensional process $\psi(t)$ has a stable equilibrium point ($\psi=0$). It is obvious that the analogy shows the basic probabilistic character of our approach; moreover it represents a suggestive and intuitive counterpart of a pure probabilistic description, offering at the same time a great body of analytic tools applicable to our problem.

As a matter of fact, if the term F_1 describing the fly's induced response in Eq. (3) is a linear one, the well-known correlation method makes it easy to find a complete solution of the problem. If, however, F_1 is nonlinear, considerable difficulties arise. One method which often enables one to carry out an exact analysis of problems of this kind is the Fokker-Planck method, which actually makes use of the quasi-brownian analogy [see for instance Wax (1954)]. The associated Fokker-Planck partial differential equation will be considered later and discussed for some simple cases.

3.4. Experimental Evidence for a Linear Approach

An experiment has been performed in order to test the form of Eq. (3) and some of its underlying assumptions. Moreover the experiment tests the hypothesis that $F_1(\psi,\dot{\psi})$ can be approximated by a linear relation when a single-stripe pattern is fixated under low coupling conditions. The latter implies that the ψ, $\dot{\psi}$ fluctuations are small. Since L is a linear system, the overall transfer function $G(f)$ of the closed loop scheme, given in Fig. 6, consequently is a linear one. Taking into account that $N(t)$ is a random process, the following relation for the power spectra holds

$$\phi(f)=\tilde{N}_0(f)\cdot|G(f)|^2 \quad (4)$$

where $\phi(f)$ designates the power spectrum of $\psi(t)$ and $\tilde{N}_0(f)$ the power spectrum of the noise.

The experimental test consists in the application of an independent zero-mean noise source, during a stripe fixation test $\left(\text{the coupling amounted to } \frac{\Theta}{k}=8\cdot10^{-3}\,\text{sec}\right)$, whose frequency band covers about the same range as the torque signal generated by the fly. The independent noise is added to the output of the

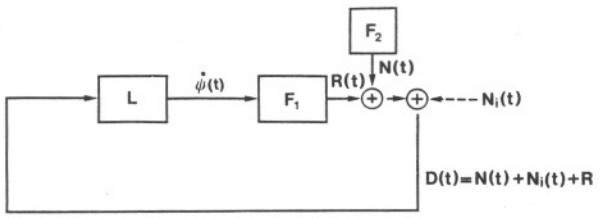

Fig. 7. The same information flow diagram as given in Fig. 6 when artifical torque noise $N_i(t)$ is added to the noise process $N(t)$ generated by the fly

torque compensator signal, as shown schematically in Fig. 7. From our experimental conditions it follows that

$$\tilde{N}_0(f) = \tilde{N}(f) + \tilde{N}_i(f) . \tag{5}$$

Substituting $\tilde{N}_0(f)$ in Eq. (4) and integrating $\phi(f)$, it follows that

$$\int_{-\infty}^{+\infty} \phi(f)\, df = \int_{-\infty}^{+\infty} df \{\tilde{N}(f) \cdot |G(f)|^2 + \tilde{N}_i \cdot |G(f)|^2\} . \tag{6}$$

During the experiment the independent noise amplitude can be changed. We therefore introduce here an amplitude scaling factor n, so that $\tilde{N}_i(f) = n^2 \tilde{N}_{i,\,\mathrm{const}}(f)$. Taking into account that

$$\int_{-\infty}^{+\infty} \phi(f)\, df = \sigma^2 , \tag{7}$$

where σ designates the standard deviation of the gaussian probability distribution of a stripe position under fixation, we arrive at

$$\sigma^2 = \sigma_0^2 + n^2 \sigma_{i,\,\mathrm{const}}^2 , \tag{8a}$$

with

$$\sigma_0^2 = \int_{-\infty}^{+\infty} \tilde{N}(f)\, |G(f)|^2\, df \tag{9}$$

and

$$\sigma_{i,\,\mathrm{const}}^2 = \int_{-\infty}^{+\infty} \tilde{N}_{i,\,\mathrm{const}}(f)\, |G(f)|^2\, df . \tag{10}$$

From Eq. (8a) it follows that

$$\sqrt{\sigma^2 - \sigma_0^2} = n \cdot \sigma_{i,\,\mathrm{const}} . \tag{8b}$$

Therefore, if our assumptions are valid, the linear relation expressed in Eq. (8b) should be fulfilled in a stripe fixation experiment.

Figure 8 contains a typical experimental test for Eq. (8b) under the conditions of low coupling. As one can see, relation (8b) is very precisely fulfilled. The result is therefore in accordance with the assumptions stated before.

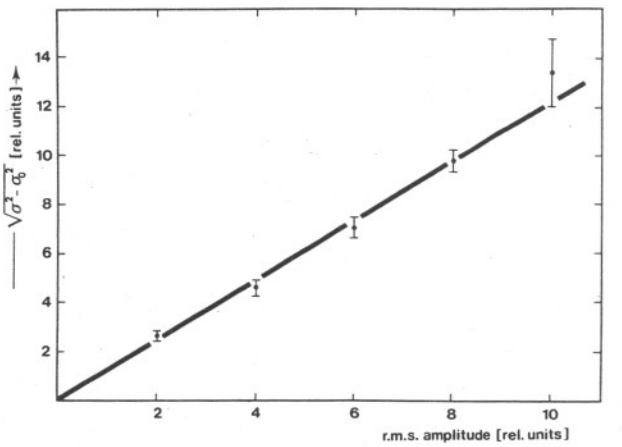

Fig. 8. Typical experimental relationship between the standard deviations σ of the fixation histogram and the power (in arbitrary units) of the artificial gaussian noise injected additively into the closed loop (see Fig. 7). The quantity σ_0 represents the standard deviation of the fixation histogram without artificial noise. The points are averages taken from five flies; the correlation coefficient $r = 0.997$. Removing the last point, where the associated histograms begin to differ from a gaussian, r becomes 0.999. The artificial gaussian noise used in this experiment had a flat spectrum up to 15 Hz where a sharp cutoff takes place. Other spectra were used too and always led to a linear relationship

3.5. A Linear Approximation

Due to the fact that a test-fly fixates a single black stripe, we may say that the stripe during the stationary fixation phase is positioned in an equilibrium state. This observation in connection with the experiment reported in Section 3.4 leads to the most obvious approach to a linearisation of Eq. (3) since it describes a system in the neighborhood of an (stable) equilibrium. Without the noise term, the equilibrium of the system in the phase space is defined by

$$\psi_{\mathrm{equil.}} = 0 ; \quad \left(\frac{d\psi}{dt}\right)_{\mathrm{equil.}} = 0 . \tag{11}$$

As long as $\overline{\psi^2}$ and $\overline{\dot{\psi}^2}$ are small enough, which is the case for low coupling, the motion of the phase point, representing the stripe, is restricted to the neighborhood of the point of equilibrium. Under these circumstances we may replace $F_1\{\psi(t'); \dot{\psi}(t')\}$ by its linear approximation near the equilibrium

$$F_1\{\psi(t'); \dot{\psi}(t')\} \approx F_1(0,0) + \left(\frac{\partial F_1}{\partial \psi}\right)_{0,0} \cdot \psi(t') + \left(\frac{\partial F_1}{\partial \dot{\psi}}\right)_{0,0} \cdot \dot{\psi}(t') . \tag{12}$$

Taking into account that $F_1(0, 0) = 0$ (equilibrium) and defining

$$\left(\frac{\partial F_1}{\partial \psi}\right)_{0,0} = \alpha \quad \text{and} \quad \left(\frac{\partial F_1}{\partial \dot{\psi}}\right)_{0,0} = r \tag{13}$$

we arrive at

$$F_1(\psi, \dot{\psi}) \approx \alpha \psi(t') + r\dot{\psi}(t'). \tag{14a}$$

Taking into consideration this linearisation, we may now reformulate Eq. (3);

$$\ddot{\psi}(t) + \frac{k}{\Theta}\dot{\psi}(t) = \frac{1}{\Theta}N(t) - \frac{\alpha}{\Theta}\cdot\psi(t') - \frac{r}{\Theta}\dot{\psi}(t'). \tag{15}$$

In this connection one has to be aware of the fact that the expression given in Eq. (14a), and consequently in (15), is the simplest linear form, *neglecting* the ψ-dependence of r as well as the $\dot{\psi}$-dependence of α. The linearisation fails when the stripe does not move relative to the compound eyes of the fly.

It might be interesting to note that Eq. (14a) can be considered a particular case (for the neighborhood of $\psi = 0$) of the more general formula

$$F_1(\psi, \dot{\psi}) = r\dot{\psi} - D(\psi), \tag{14b}$$

where the difference between the progressive and the regressive induced torque response is now described by the experimentally given function $D(\psi)$ for the ψ-range $-\pi < \psi \leqq +\pi$. Formally, Eq. (14b) can then be rewritten as

$$F_1(\psi, \dot{\psi}) = r\dot{\psi} + \frac{\partial}{\partial \psi}U(\psi), \tag{14c}$$

where $D(\psi)$ is supposed to be derived from a potential $U(\psi)$. It is clear that the term $\alpha\psi(t')$ in Eq. (14a) describes the linear range of $D(\psi)$ between about $-20°$ and $+20°$. For this region, Eq. (14b) reduces to (14a). Both functions, $D(\psi)$ and $U(\psi)$, are presented in Fig. 9.

The standard linearisation applied here is typical for non-stochastic processes. The fact, however, that we are dealing with stochastic processes justifies the procedure also from the point of view of statistical linearisation; Kasakov (1961).

Another argument speaking in favour of a linear approximation comes from the experimental evidence; namely that the distributions (histograms) characterizing the closed-loop fluctuations are quite well approximable by *normal* distributions when the coupling is low. In fact it is well known that if one injects a normal process into a closed-loop system containing a nonlinear element, the variables of the system, in general, fluctuate in a nongaussian manner. Therefore,

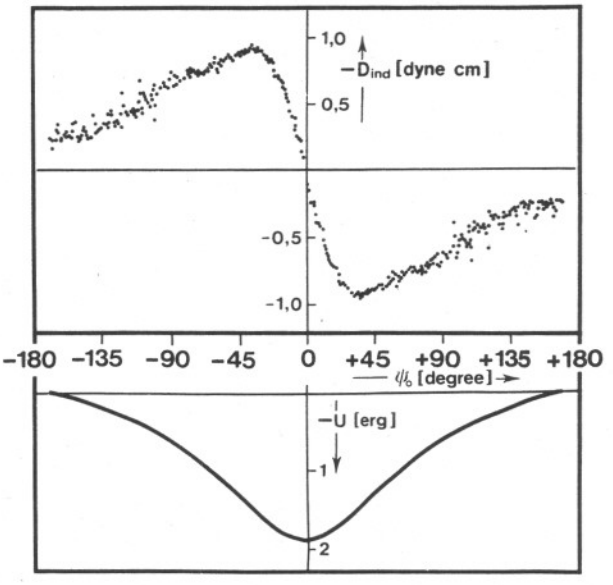

Fig. 9a. The asymmetric part of the torque induced by a moving stripe as a function of the angular position ψ_0; average of 111 single measurements. In these measurements the flies were coupled $\left(\frac{\Theta}{k} = 12 \cdot 10^{-3}\right)$ to a panorama containing a black vertical stripe of width 5° which was elastically bound to each angular position ψ_0. The average rotation speed was 1°/sec, too low to produce any significant reaction. The experiment measures $D(\psi) = -\overline{F_1(\psi, \dot{\psi})}$ where the bar indicates an average for each ψ with respect to the actual closed loop zero-mean speed distribution. It is natural to approximate $F_1(\psi, \dot{\psi})$ as $F_1(\psi, \dot{\psi}) \cong r\dot{\psi} - D(\psi)$ when the speed fluctuations around $\dot{\psi} = 0$ are small – i.e. for low coupling conditions. When $\overline{\psi^2}$ is also small, as in the case of single stripe patterns, the motion of the stripes is confined to the linear region of $D(\psi)$, and then $F_1(\psi, \dot{\psi}) \cong r\dot{\psi} + \alpha\psi$

Fig. 9b. The potential profile $U(\psi)$ for single vertical stripes obtained from the experimental $D(\psi)$ (Fig. 9a) according to the usual definition of $D(\psi) = -\operatorname{grad} U(\psi)$. The potential always exists since $D(\psi)$ is a one dimensional function. The minima of $U(\psi)$ give the stable fixation positions

we may conclude that the linearized description of the fixation process is a reasonable one.

Equation (15) is a linear equation of the *Langevin* type, which describes the stochastic process $\psi(t)$. Since $N(t)$ is gaussian $\psi(t)$ also must be a *normal* random process. It follows from Eq. (15) that the power spectrum $\Phi(f)$ of $\psi(t)$ is given by the expression

$$\Phi(f) = \frac{\frac{1}{\Theta^2}\cdot\tilde{N}(f)}{\left|-4\pi^2 f^2 + i2\pi f\left\{\frac{k}{\Theta} + \frac{r}{\Theta}e^{-i2\pi f\varepsilon}\right\} + \frac{\alpha}{\Theta}e^{-i2\pi f\varepsilon}\right|^2}, \tag{16a}$$

where $\tilde{N}(f)$ again designates the power spectrum of $N(t)$. Since the process $\psi(t)$ is normal, it is completely determined by its mean and its autocorrelation function. The autocorrelation $S_{\psi,\psi}|\tau|$ can be obtained either directly from the inverse Fourier transform of the power spectrum $\Phi(f)$, or by performing the following convolution operation

$$S_{\psi,\psi}(\tau)=\frac{1}{\Theta^2}(S_{T,T}*S_{N,N}), \tag{17a}$$

where $S_{N,N}$ describes the autocorrelation of the noise and $S_{T,T}$ the Inverse-Fourier-Transform of the denominator term in Eq. (16a).

Unfortunately it is not possible to obtain, in general, an analytic expression for $S_{T,T}$, due to the finite delay time ε. However, in the frame of our approximation it seems even possible to neglect ε for the case of low couplings between the fly and its surroundings, see Appendix A. This is also suggested by the outcome of the experiment described before (Section 3.4), which implies a negligible delay. In the following we shall therefore neglect the delay ε of the induced response F_1. Equation (16a) reduces then to

$$\Phi(f)=\frac{\frac{1}{\Theta^2}\cdot\tilde{N}(f)}{\left|-4\pi^2 f^2+i2\pi f\left(\frac{k}{\Theta}+\frac{r}{\Theta}\right)+\frac{\alpha}{\Theta}\right|^2}. \tag{16b}$$

We are now able to develop a straightforward analytical expression for $S_{T,T}$ in Eq. (17a). Introducing the following abbreviations,

$$b=\frac{k}{\Theta}+\frac{r}{\Theta};\quad a=\frac{\alpha}{\Theta};\quad 2\pi f^*=\sqrt{a-\frac{b^2}{4}}, \tag{18}$$

we arrive at

$$S_{T,T}(\tau)=\frac{1}{2ab}e^{-\frac{b}{2}|\tau|}\left[\cos 2\pi f^*\cdot\tau+\frac{b}{4\pi f^*}\sin 2\pi f^*|\tau|\right]. \tag{17b}$$

$S_{T,T}(\tau)$ behaves oscillatory, aperiodic, or overdamped, according to whether f^* is real, zero, or imaginary.

For the second term $S_{N,N}$ in Eq. (17a), which undergoes convolution with $S_{T,T}$, the analytical expression approximating our measurements in open-loop conditions (see Fig. 4b) is given by

$$S_{N,N}(\tau)=A\,e^{-\gamma|\tau|}. \tag{19}$$

Under the assumption that the open-loop noise is representative of the noise process generated by the fly under closed-loop conditions (see Appendix A), we are now in a position to determine $S_{\psi,\psi}(\tau)$ in Eq. (17a) by convoluting the expressions for $S_{T,T}$ and $S_{N,N}$, given in Eqs. (17b) and (19). The result of the calculation is derived in Appendix B; the special case $\tau=0$ is given in the next equation

$$S_{\psi,\psi}(0)=\sigma^2=\frac{A}{\Theta^2\cdot a\cdot b}\cdot\frac{b+\gamma}{(a+b\cdot\gamma+\gamma^2)}. \tag{20}$$

The stationary probability distribution of the stripe position ψ is, since $\bar{\psi}=0$, given by the following gaussian expression

$$P(\psi)=\sqrt{\frac{1}{2\pi\sigma^2}}\,e^{-\frac{\psi^2}{2\sigma^2}}. \tag{21}$$

It follows from Eq. (20) that σ^2 is proportional to A, which represents the power of the torque fluctuation introduced in Eq. (19). On the other hand σ^2 is inversely related to the parameter a which designates the slope of the $D(\psi)$-characteristics in the linear region near $\psi=0$, see Fig. 9.

This dependence upon the parameter a clearly means that fixation is in principle guaranteed only if the value of a is different from zero. The parameter b in Eq. (20), which has been specified in Eq. (18), consists of two terms: The first one $\frac{k}{\Theta}$ represents the coupling of the fly to the panorama, whereas the second one $\frac{r}{\Theta}$ designates the symmetric part of the torque response induced by the moving pattern. In the "white" noise approximation ($\gamma\to+\infty$; $A\sim\gamma$), σ^2 is inversely proportional to a and b since A times the second part of the equation containing a, b and γ [see Eq. (20)] reduces to unity. The σ^2 dependence upon b is quite understandable, as it determines the speed-sensitive open-loop amplification of the entire control system.

In Fig. 10 a sequence of fixation distributions for a single stripe has been derived from Eqs. (20) and (21), taking into account actual values for the parameters k, A, a, b and γ. These values are specified in the legend of the figure. Comparing the calculated distributions in Fig. 10 with the measured distributions presented in Fig. 2, one can easily see that Eq. (20) fails, as expected, at high couplings, where the assumptions under which the linearisation was derived are no longer valid (see Appendix A).

In a recent paper, one of us (Reichardt, 1973) has reported that fixation of elementary objects like stripes is confined to the lower halves (below the equators) of the compound eyes. Therefore we have to assume that the parameter a in Eq. (20) is different

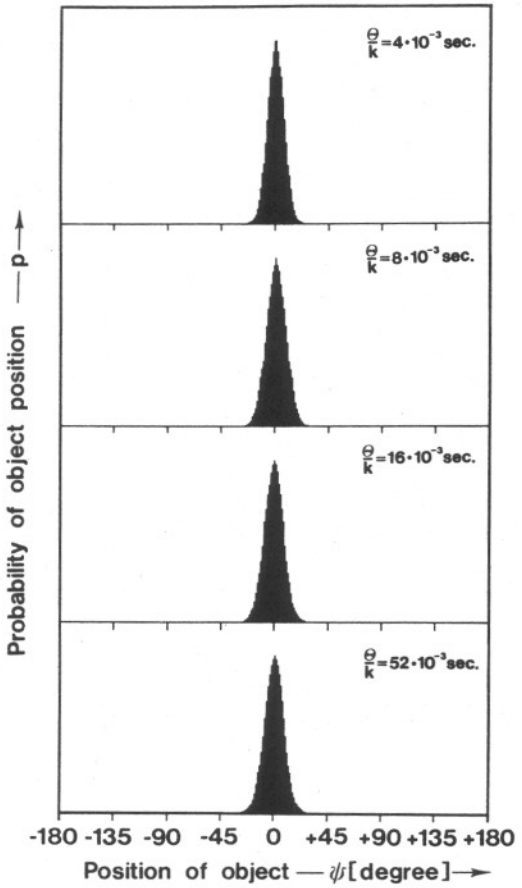

Fig. 10. Theoretically derived probability distributions representing the stationary phase of fixation of a black vertical stripe, plotted by the computer according to Eq. (21). The parameters A and γ are derived from Fig. 4a and 4b in which $\sqrt{A}\cong 0.3$ [dyne · cm], $\gamma\cong 1.9$ [sec^{-1}]. The value of $a=\frac{\alpha}{\Theta}$, determined by the slope of the linear $D(\psi)$ region, is given by Fig. 9, where $a\cong 1300$ [sec^{-2}]. The parameter r, which has not been measured experimentally, is given a value which produces histograms typical of those experimentally obtained for low coupling. The probability distributions compare well with the experimental ones of Fig. 3, for low coupling. The high coupling $\left(\frac{\Theta}{k}=52\cdot10^{-3}\right)$ distribution is given here to show the expected failure of the linearized equations in these conditions (associated with high values of $\overline{\dot{\psi}^2}$ and $\overline{\psi^2}$)

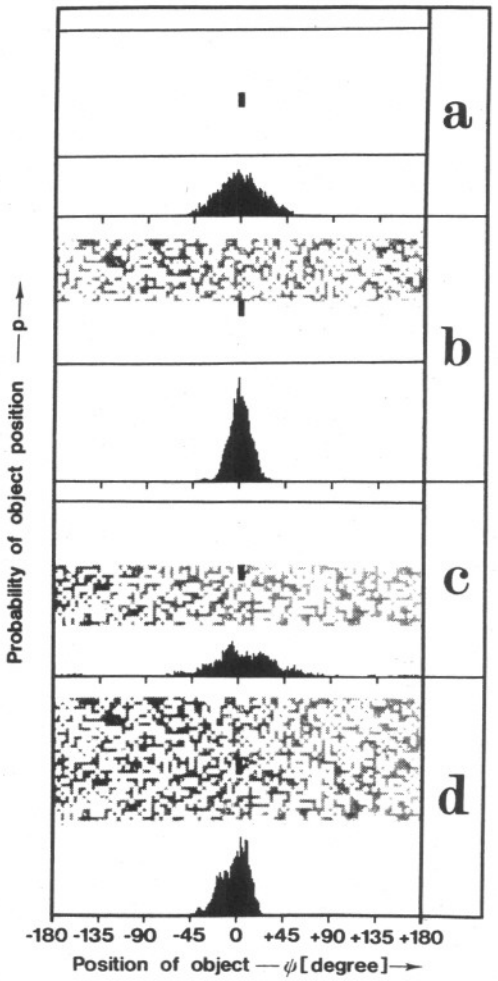

Fig. 11. Fixation of a stripe segment in the presence and absence of contrast visual noise (average contrast 50%). The figures a–d show in the upper part the patterns and in the lower the corresponding stationary fixations. The results, from a single test fly, are qualitatively typical. The value of the coupling parameter is $\frac{\Theta}{k}=8\cdot10^{-3}$ [sec]. For further explanation see the text

from zero in the lower regions, whereas in the upper regions of the eyes a should be equal to zero. Concerning the induced symmetric torque response which is partly represented by the parameter b, it is about homogeneously distributed in horizontal eye regions above and below the equators of the compound eyes, as has been shown by Götz (1964) for *Drosophila*. In addition it is known that induced torque responses elicited in different parts of the eyes contribute additively to the total response, Reichardt (1973). Consequently, the result given in Eq. (20) should be applicable even to those special experimental cases where the lower parts of the eyes are confronted with a pattern different from the upper parts.

In Fig. 11 we report the outcome of a typical experiment. Fig. 11a illustrates the case when a single stripe segment is positioned just below the equatorial line of the two compound eyes, resulting in the fixation of the segment, shown in the lower section of Fig. 11a. In the following experiment the upper part of the panorama contains visual noise of medium contrast (about 50%). As can be seen in the lower portion of Fig. 11b, the presence of the visual noise in the upper part of the panorama clearly improves the quality

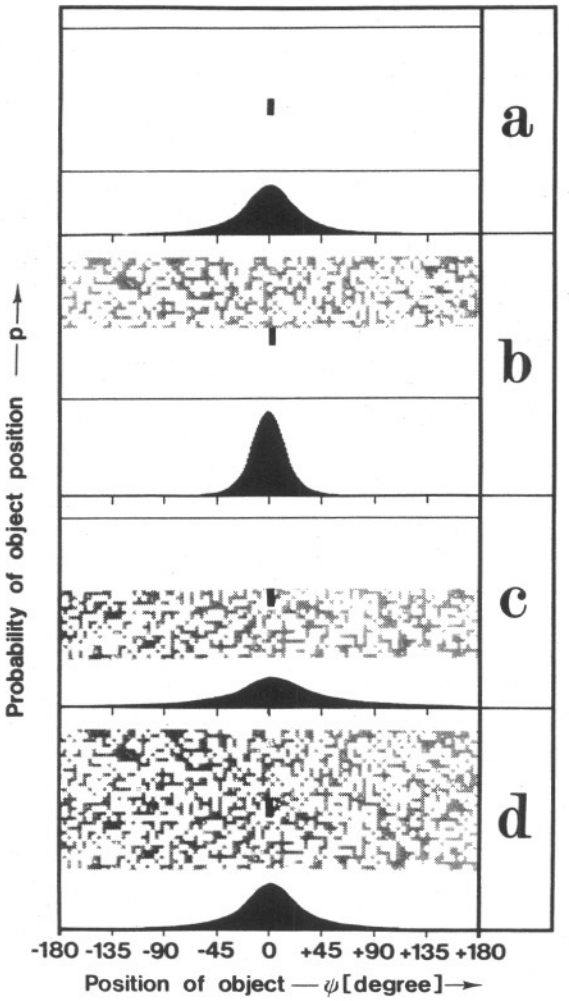

Fig. 12. The theoretically derived probability distributions for the experiment of Fig. 11 obtained from Eq. (21) and plotted by a computer. The (exemplifying) values of the parameters are those used in Fig. 10 (or obtained from them as explained in the text). The nonlinear shape of $D(\psi)$ (see Fig. 9) is taken into account in these plots. Equation (31) is used to find the equivalent "white" noise spectral density which in the linear region of $D(\psi)$ gives the same σ as that of Eq. (21); the equivalent spectral density is then used in Eq. (31) to give an approximate probability distribution over the whole range. The probability distributions a–d show a good agreement with the typical behavior of the flies (see Fig. 11)

of the fixation of the stripe segment. If, however, as in the next experiment, the visual noise covers the lower part of the panorama, a marked decrease in the fixation quality is observed, as can be seen in Fig. 11c. In the following experimental case, where the contrast noise covers the entire panorama, fixation is improved again to about the same quality as in the first experiment when only the stripe segment was presented. This is shown in Fig. 11d.

We have theoretically derived the outcome of the experimental results shown in Fig. 11 by calculating a sequence of histograms from Eqs. (20) and (21); the results are presented in Fig. 12. In connection with these calculations, we took the nonlinear shape of the $D(\psi)$-characteristics into account (see legend of Fig. 12). The quantitative details of the calculations rest on sample numerical values of the parameters in Eq. (20) which were derived from other experiments. For the experiments reported in Fig. 11, the coupling amounted to $\frac{\Theta}{k} = 8 \cdot 10^{-3}$ [sec]. The numerical values of the parameters A and γ were determined in open loop experiments presented in Figs. 4a and 4b; they are of the order, $\sqrt{A} \simeq 0.3$ [dyne · cm] and $\gamma = 1.9$ [sec^{-1}]. Parameter a was derived from the 111 superimposed $D(\psi)$-characteristics shown in Fig. 9 by taking into consideration that the stripe segment covered only about 25% of the lower half of the panorama. Under these conditions the estimate for a amounts to about $a = 450$ [sec^{-2}]. The numerical value of the parameter b, which amounts to $b = 135$ [sec^{-1}], is derived from the $\sigma^2 \approx 0.13$ [rad^2] value of the fixation distribution generated by the black stripe segment in Fig. 11a. The value given here for b is consistent with the value assumed for r in connection with the results reported in Fig. 10, if one takes into account the different sizes of the stripes. According to these numerical values of the parameters, a fixation distribution was calculated from Eqs. (20) and (21) and is shown in Fig. 12a. This distribution is the theoretically derived counterpart of the fixation distribution presented in Fig. 11a. In Fig. 11b we reported the fixation behavior of a test fly to the stripe segment under the influence of a noise pattern of about 50% contrast positioned in the upper part of the panorama. Under these pattern conditions, the number of receptors receiving contrast signals is increased by about a factor 40 compared to the original pattern consisting of the stripe segment only. Since at high brightness levels, at which these experiments have been carried out, 50% contrast is nearly as efficient as 100% contrast, one has to expect that the parameter r is increased roughly by the factor 40, which in turn affects the parameter b in Eq. (20) and reduces σ^2 to a value of $\sigma^2 \approx 0.05$ [rad^2]. The corresponding fixation distribution is plotted in Fig. 12b; it is in good agreement with the experimental one presented in Fig. 11b. In Fig. 11c we reported the result of a fixation experiment when the visual noise covered the lower part of the panorama. Under these pattern conditions, a remarkable reduction in the quality of the fixation was observed. Since there is experimental evidence suggesting that the strength of

the symmetric induced torque response from the upper parts of the compound eyes equals those from the lower parts, we can assume that the numerical value of the parameter r is about the same in both cases when the contrast noise covers either the upper half or the lower half of the panorama. Consequently it seems logical to infer that the numerical value of the parameter a has to be decreased in order to match the theoretically determined histogram with the experimental result which shows reduced fixation quality. As has been stated before, there is good experimental evidence that the contributions to the induced torque response elicited from different regions of the eyes summate linearly and, conversely, that each contrast element makes its own independent contribution to the overall potential profile, Reichardt (1973). Under these conditions the upper level of the potential profile is decreased compared to the level generated by the stripe segment alone. This in turn reduces the relative depth of the potential hole, which corresponds to saying that the numerical value of the parameter a is reduced. A fitting of the histogram of the measured fixation distribution given in Fig. 11c requires a reduction in a by about a factor of three ($\sigma^2 \approx 0.23$), which leads to the calculated distribution plotted in Fig. 12c. In the last case, the visual noise covers the entire panorama and leads to the experimental result plotted in Fig. 11d. The corresponding theoretically derived histogram was calculated with the numerical values for the parameters given before, except for r which must take twice the value since the visual noise covers the lower *and* the upper half of the panorama. The result is presented in Fig. 12d.

In summary we can state: There is so far good agreement between the experimental and the calculated results, which shows that our theory does not only apply to fixation under elementary conditions but also to the behavior elicited by those patterns which require an independent change of the values of the parameters a and b.

In Section 3.3 we have pointed out that our theoretical description of the pattern fixation process is mathematically similar to the quasi-brownian motion of a particle in a potential hole. In this picture, the application of visual noise to the upper part of the panorama is equivalent to an increase of the particle's friction on its path in the neighborhood of the potential minimum. The influence of the friction results in a narrowing of the particle's position distribution compared to the distribution generated without friction. If, on the other hand, in our experiments the visual noise is positioned in the lower part of the panorama, its influence is equivalent to a decrease in the depth of the potential hole generated by the stripe segment. This influence overrides the effect of the friction. When however the visual noise covers the entire panorama both effects about compensate each other.

3.6. A More General Mathematical Treatment

The theory developed so far is a linear approximation of a more general case [Eq. (3)], valid only if the position and speed fluctuations are small, which is experimentally realized during the fixation of a single stripe under low coupling conditions. In the following we shall outline a more general approach for a solution of the nonlinear Langevin-equation (3) which is based on a formalism known in physics as the Fokker-Planck method. The application of the method seems appropriate to describe and to predict those orientation (fixation) experiments where the panorama carries a pattern which consists of more than one stripe.

Rewriting the expression for the generalized Langevin equation (3)[2] in the phase space (ψ, w), we arrive at

$$\begin{aligned} \frac{d\psi}{dt} &= w \\ \frac{dw}{dt} &= \frac{N(t)}{\Theta} - \frac{k}{\Theta} w - \frac{F_1}{\Theta}(\psi, w)\,. \end{aligned} \tag{22}$$

The procedure of solving these equations is simplified if we assume that the stationary, gaussian noise process $N(t)$ is "white". This assumption enables us to obtain approximate solutions which however contain the main features of the given problem. One can show (see Appendix C) that the non-"white" noise case is well approximated by the "white" noise assumption if the coupling is low and the strength of the induced torque response large compared to the maximum slope of the potential. Another possibility of approximating experimentally the "white" noise condition is to add to the fly's torque response gaussian "white" noise from a noise generator whose power is large compared to the fly's noise.

In the following we set up the Fokker-Planck-equation, which in general is given by the expression

$$\begin{aligned} \frac{\partial p}{\partial t} = &- \frac{\partial}{\partial \psi}[A_1(\psi, w) \cdot p] - \frac{\partial}{\partial w}[A_2(\psi, w) \cdot p] \\ &+ \frac{1}{2}\left[2\frac{\partial^2}{\partial w\, \partial \psi}(B_{12} \cdot p) + \frac{\partial^2}{\partial w^2} B_{22} p + \frac{\partial^2}{\partial \psi^2} B_{11} \cdot p\right], \end{aligned} \tag{23}$$

[2] In the following we neglect again the delay time in the fly's reaction, which is permissible in the cases of low coupling (see Appendix A).

where

$$A_1 = \lim_{\Delta t \to 0} \frac{\langle \Delta \psi \rangle^*}{\Delta t},$$

$$A_2 = \lim_{\Delta t \to 0} \frac{\langle \Delta w \rangle}{\Delta t},$$

$$B_{11} = \lim_{\Delta t \to 0} \frac{\langle \Delta \psi^2 \rangle}{\Delta t},$$

$$B_{12} = \lim_{\Delta t \to 0} \frac{\langle \Delta w \Delta \psi \rangle}{\Delta t},$$

$$B_{22} = \lim_{\Delta t \to 0} \frac{\langle \Delta w^2 \rangle}{\Delta t}.$$

The values of the coefficients A_1 through B_{22} are determined from Eq. (22), which finally lead to the following expression for the Fokker-Planck equation;

$$-\frac{\partial}{\partial \psi}(w \cdot p) + \frac{\partial}{\partial w}\left[\frac{F_1}{\Theta} + \frac{k}{\Theta} \cdot w\right] \cdot p + \zeta \frac{\partial^2 p}{\partial w^2} = \frac{\partial p}{\partial t} \quad (24)$$

where $\zeta = \frac{c}{\Theta^2}$, $S_{N,N}(\tau) = 2c\delta(\tau)$ and $p = p(\psi, w | \psi_0, w_0; t)$.

As has been pointed out before, we assume here that the torque fluctuation is stationary and F_1 is not dependent on t. Equation (24) is a general expression which holds for different forms of F_1. For low coupling conditions (small $\overline{\dot{\psi}^2}$) we may approximate $F_1(\psi, \dot{\psi})$ by

$$F_1(\psi, \dot{\psi}) \cong r\dot{\psi} + \frac{\partial}{\partial \psi} U(\psi), \quad (25)$$

where $U(\psi)$ designates a ψ-dependent cyclic potential associated with the asymmetric part of the induced torque response. The potential for a single stripe is presented in Fig. 9b. If a pattern consists of an ensemble of vertical stripes, one can apply the "superposition rule" (see Reichardt, 1973) in order to derive the associated potential, which is established by the superposition of the individual potentials generated by individual stripes.

Taking into account these properties of $U(\psi)$ and inserting Eq. (25) into Eq. (24) we arrive at

$$-\frac{\partial}{\partial \psi}(wp) + \frac{\partial}{\partial w}\left\{\left[b \cdot w + \frac{1}{\Theta}\frac{\partial}{\partial \psi} U(\psi)\right] p\right\} + \zeta \frac{\partial^2 p}{\partial w^2} = \frac{\partial p}{dt}. \quad (26)$$

A solution of Eq. (26) is simplified if one confines the problem to a calculation of the stationary position probability $p(\psi)$ which is theoretically approximated by experiments of infinite time duration. Due to the fact that the ψ-coordinate is a cyclic one, stationarity is in our case ensured. The stationary condition requires that $\frac{\partial p}{dt} = 0$. Consequently the stable distributions

$$p(\psi, w | \psi_0, w_0) \to p_{st.}(\psi, w) \quad (27)$$

which have to satisfy the conditions

$$\begin{aligned} &p_{st.}(w, \psi) \to 0 \quad \text{for} \quad w \to \pm\infty; \\ &p_{st.}(w, \psi) = p_{st.}(w, \psi + 2n\pi); \quad n = 0, 1, \ldots, \\ &p_{st.}(w, \psi) > 0; \quad \int_{-\pi}^{+\pi} \int_{-\infty}^{+\infty} p_{st.}(\psi, w)\, dw\, d\psi = 1, \end{aligned} \quad (28)$$

are the solutions of equation

$$-\frac{\partial}{\partial \psi}(w \cdot p) + \frac{\partial}{\partial w}\left\{\left[b \cdot w - \frac{1}{\Theta}\frac{\partial}{\partial \psi} U(\psi)\right] \cdot p\right\} + \zeta \frac{\partial^2 p}{\partial w^2} = 0. \quad (29)$$

The solution for p is given by the expression

$$p(w, \psi) = C e^{-\left(\frac{w^2}{2} + \frac{U(\psi)}{\Theta}\right)\frac{b}{\zeta}}, \quad (30)$$

where C is a normalization constant. Integrating w from $-\infty$ to $+\infty$, we get

$$p(\psi) = \sqrt{\frac{\zeta \cdot \pi}{b}} \cdot C \cdot e^{-\frac{U(\psi)}{\Theta} \cdot \frac{b}{\zeta}}. \quad (31)$$

Equation (31) relates an arbitrary cyclic potential profile $U(\psi)$, generated by one or many individual stripes, to the stationary position probability $p(\psi)$ of the fly. Due to the fact that an e-function is a monotonic function, a one-to-one nonlinear relation between $U(\psi)$ and $p(\psi)$ is expressed by Eq. (31). The parameter b has in this connection a similar influence as in the visual noise experiments. An increase in b is equivalent to an enhancement whereas a decrease in b to a reduction of the potential profile. The converse holds for the parameter ζ which represents the power density of the "white" noise torque fluctuation. Further implications of Eq. (31) will be considered in the discussion.

Our next point concerns the probability of jumping from a minimum in the potential profile across the barrier of the potential wall located in the neighbourhood of one minimum. A typical portion of a potential profile, illustrating a minimum, the neighbouring slope, and a potential barrier, is given in Fig. 13. ψ_0 indicates the position of the potential minimum, ψ_b the position of the barrier maximum and $E = U(\psi_b) - U(\psi_0)$ the potential energy difference between the minimum and the maximum.

* The brackets $\langle\ \rangle$ designate the time averages.

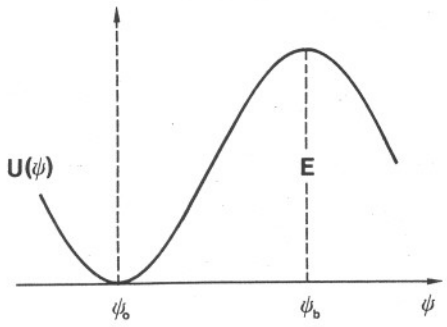

Fig. 13. Part of a potential profile $U(\psi)$ showing one minimum in the position $\psi = \psi_0$ and a "barrier" in $\psi = \psi_b$. The "height" of the barrier is $[U(\psi_b) - U(\psi_0)] = E$. When the potential profile is obtained by the "superposition rule" applied to the single stripe potential of Fig. 9, the potential $U(\psi)$ is exactly described by a harmonic potential near ψ_0 and by $[E - 1/2\alpha'(\psi - \psi_b)^2]$ near ψ_b

We are considering here that an escape of the "particle" from the potential hole is a not too frequent event, in order to guarantee quasi-stationary. This assumption is specified by the condition $E \gg \frac{\zeta \Theta}{b}$. Because of the shape of the $D(\psi)$ characteristics generated by a single stripe, it is possible to describe the potential hole and the neighbouring barrier by two quadratic (harmonic) expressions. Even an arbitrary potential profile can be approximated piecemeal by such harmonic potentials. Consequently the expression for the potential profile around a minimum is given by

$$\frac{U(\psi)}{\Theta} = \frac{1}{2} a(\psi - \psi_0)^2 , \tag{32}$$

and near a maximum by

$$\frac{U(\psi)}{\Theta} = \frac{E}{\Theta} - \frac{1}{2} a'(\psi - \psi_b)^2 . \tag{33}$$

Inserting these expressions for $U(\psi)$ into Eq. (26), we arrive at

$$0 = +a\psi \frac{\partial p}{\partial w} - w \frac{\partial p}{\partial \psi} + b \frac{\partial}{\partial w} \cdot w \cdot p + \zeta \frac{\partial^2 p}{\partial w^2} \text{ near } \psi_0, \tag{34}$$

and

$$0 = -a'\psi' \frac{\partial p}{\partial w} - w \frac{\partial p}{\partial \psi'} + b \frac{\partial}{\partial w} w \cdot p + \zeta \frac{\partial^2 p}{\partial w^2} \text{ near } \psi_b , \tag{35}$$

where $\psi' = (\psi - \psi_b)$, $\psi_0 = 0$.

The solutions of the Eqs. (34), (35), which are derived in detail in Appendix D, are given by the following expressions

$$p_{\text{near } \psi_0}(\psi, w) = C \cdot e^{-(w^2 + a\psi^2) \cdot \frac{b}{2\zeta}} \tag{36}$$

$$p_{\text{near } \psi_b}(\psi', w) = C \cdot \left(\frac{\mu - b}{2\pi\zeta} \right)^{1/2} \cdot e^{-\frac{E \cdot b}{\Theta \zeta}} \cdot e^{-(w^2 - a'\psi'^2) \cdot \frac{b}{2\zeta}} \cdot \int_{-\infty}^{\varrho} e^{-(\mu - b)\frac{\varrho^2}{2\zeta}} d\varrho \tag{37}$$

where $\varrho = w - \mu\psi'$ and $\mu = \frac{b}{2} + \sqrt{\frac{b^2}{4} + a'}$.

The probability flow of a "particle" (stripe) across the barrier is

$$j'_b = \int_{-\infty}^{+\infty} p_b(\psi' = 0, w)\, w\, dw , \tag{38}$$

from which, integrating by parts, we obtain (see Appendix *D*) the expression

$$j'_b = C \left(\frac{\mu - b}{\mu} \right)^{1/2} \frac{\zeta}{b} e^{-\frac{E \cdot b}{\Theta \zeta}} . \tag{39}$$

A normalization procedure for one particle (stripe), carried out through Eq. (36), leads to a determination of $C = \frac{\sqrt{a \cdot b}}{2\pi\zeta}$. In connection with Eq. (39) we finally get for the probability per unit time that a stripe escapes the potential hole across ψ_b

$$p_{b_{\text{escape}}} = \frac{\sqrt{a}}{2\pi} \sqrt{\frac{\mu - b}{\mu}}\, e^{-\frac{Eb}{\zeta\Theta}} = \frac{\sqrt{a}}{2\pi\sqrt{a'}} \left(\sqrt{\frac{b^2}{4} + a'} - \frac{b}{2} \right) \cdot e^{-\frac{Eb}{\Theta \cdot \zeta}} . \tag{40}$$

Experimentally we usually have $\frac{b^2}{4} \gg a'$, which simplifies Eq. (40) and leads to the approximation

$$p_{b_{\text{escape}}} \approx \frac{1}{2\pi(k + r)} \sqrt{\alpha \cdot \alpha'}\, e^{-\frac{(k+r)E}{c}} , \tag{41}$$

where $\alpha = a\Theta$ and $\alpha' = a'\Theta$.

It should be pointed out again that Eq. (41) was derived under the assumption that the torque fluctuation can be approximated by gaussian "white" noise. In the actual experiment this however is not the case. Therefore the problem has been taken up again in Appendix C and solved for a non-"white" noise spectrum. Instead of Eq. (41) we arrived at the following expression for p_b under the assumption of gaussian low-pass filtered torque noise

$$p_{b_{\text{escape}}} = \frac{1}{2\pi} \sqrt{1 + \frac{\alpha}{(k + r)\gamma}} \sqrt{\alpha \cdot \alpha'}\, e^{-\frac{\gamma(k+r)E}{A}} . \tag{42}$$

It can be easily seen that Eq. (42) reduces to the expression given in Eq. (41) when the low-pass noise approximates "white" noise (see Appendix C). For the experimentally given one-stripe case, the following numerical values are typical: $\gamma = 1.9$ [sec^{-1}], $\sqrt{A} = 0.3$ [dyne · cm], $\alpha = 2.86$ [dyne · cm], $\alpha' = 0.35$ [dyne · cm], $\frac{\Theta}{k} = 8 \cdot 10^{-3}$ [sec], $\frac{r}{\Theta} = 60$ [sec^{-1}], $E = 1.6$ [erg]. These values, inserted into Eq. (42), lead to $p_{b_{escape}}$ of $1.666 \cdot 10^{-4}$ [sec^{-1}], which amounts to an average fixation life time of 50 min. Bearing in mind that the calculated value, in this numerical example, is an underestimate because of the approximations applied in Eq. (42), it is qualitatively in good agreement with all experimental evidence.

4.0. Discussion

The mathematical analysis presented here so far is a first order approximation of the mechanisms responsible for pattern fixation and discrimination by the visual system of the fly. Refinements are possible and will be made as soon as more experimental data are available. On the other hand, even at this stage it seems important to have a general understanding of the basic organization of the system and its essential features. As we have already stated in the introduction, our present theory is of a phenomenological nature, in some ways equivalent to a "thermodynamic" description of the behavior of the fly during visual orientation tasks. Indeed, precise information about the underlying neural mechanisms cannot be obtained from these behavioral experiments only. Concerning a deeper level, which would in principle be comparable with a "statistical-mechanical" approach, one of the future steps in our investigation will be to clarify how the theory describing the quantitative details of the optomotor response, Reichardt (1969b), has to be modified in order to meet the observations at the "thermodynamic" level.

Experimentally, we have shown that a stationary retinal image of an object, either illuminated with constant or with flickering light, has no significant effect on the induced torque signal of the fly. The noise torque production by the fly, therefore, seems to constitute the necessary requirement for pattern fixation since it generates relative motion between the pattern and the fly's retinae. It should be recalled here that the torque response, induced by the fly's own torque noise, is an asymmetric one with ψ-position dependence. Other investigators, as for instance Oyster (1968), have stated that movement-direction sensitive cells cannot provide position information. This argument cannot be accepted since it is obvious that asymmetrically responding motion detectors may provide the necessary requirements for position information.

In our analysis we have treated the torque noise process of the fly as a coloured gaussian process. It cannot be excluded that under other conditions this description may require some modifications. For example, in an experimental situation in which the head of the fly is free to move relative to the thorax, it may be necessary to take possible saccadic head movements into account. They could be represented in the description as arising from a stochastic point process. The corresponding mathematical approach, necessary in the case of the human eye, has already been outlined, Poggio (1973). From this it is clear that a different stochastic characterisation of the underlying random process does not qualitatively change our mathematical formulation.

Interestingly, there are a few analogies between the fly's fixation and the human eye's fixation of stationary targets. It seems that in both cases stationary retinal images are not "perceived"; in both cases we observe a continuous "noise" production (tremor and saccades in the human eye). Vasudevan *et al.* (1972) have developed a linear mathematical model, which has formal similarities with ours, in order to account for the statistical properties of small human eye movements during steady fixation of a stationary target. Other suggestive analogies can be found; for example, in the observations reported by Richards and Kaufman (1969) about tendencies for fixation of patterns by human observers. The observer's eyes point towards a position within the pattern, near the boundaries. If, however, the outlines do not exceed about 5 degrees, the spontaneous fixation point is located near the center of gravity of the pattern. Quite similarly, the average fixation position of a fly confronted with a two-stripe pattern is towards the center of gravity of the pattern if the angular separation of the stripes amounts to less than about 40 degrees, whereas the fixation is found near the boundaries (*inside* the pattern) for larger separation angles. Richards and Kaufman also report that the fixation points of human observers approximate the foci observed in the same patterns when these are seen in front of a background consisting of visual noise. They speculate, that the radial flow observed in the presence of visual noise might be due to biased motion detectors of the orientation system; objects not perfectly centered on the fovea would create asymmetric velocity components. The analogy to our observations, Reichardt (1973), concerning the fly's asymmetry in the detection of motion might be of interest in this context.

Besides the possibilities of applying our results and considerations concerning pattern fixation to biological systems other than flies, we would like to

mention here some obvious extensions of the present theory. The first one concerns the description of the fly's behavior under visual tracking tasks. Preliminary results, Virsik (1973), indicate that the theory predicts quantitatively the average tracking characteristics for a number of different experimental conditions. For example, if an object moves with constant speed in front of a contrasted background, the fly may follow the object with an average phase lag (shift) which depends upon the induced torque response generated by the background. The quantitative details of these observations can be derived from the theory by a modification of Eq. (15). A second extension involves fixation of a vertically moving horizontal stripe, which is controlled by the fly's induced flight lift response, Wehrhahn (1973). The general properties of the control mechanisms involved here seem to allow a similar formal treatment to the one given in this paper.

The next logical step, both experimentally and theoretically, in the analysis of pattern fixation and discrimination will be to take into consideration from the dynamical point of view the other degrees of freedom. This extension of the present treatment of the problem is likely to be non-trivial if the reaction of the fly reveals couplings between the independent directions of movement.

It is obvious that the basic problem is to characterize the induced reaction F_1 for arbitrary patterns. For given low coupling parameters and noise process, it seems possible to split the induced reaction term into a symmetric optomotor response and a "potential" profile – both pattern dependent. When the pattern can be approximated by vertically oriented black stripes or stripe segments – in the presence or absence of contrast noise – these two terms are readily obtained. The additivity of the induced partial responses from the various stimulated eye regions leads to an approximate estimate for the first term, which can be further linearized for low couplings. The potential profile $U(\psi)$ associated with the pattern is obtained by the superposition of individual potential distributions, each of which is generated by an individual stripe or stripe segment, Reichardt (1973). Once F_1 is known, the associated Fokker-Planck equation gives the probability distribution which completely characterizes the spontaneous pattern discrimination behavior of the fly. In the simplified case treated in Section 3.6, the transformation pattern/orientation (fixation) has been obtained from Eq. (31) under stationary conditions. The probability distribution $p(\psi)$ characterizes the process $\psi(t)$, which is a projection of the Markov process (ψ, w) which contains the full information present at the fly's torque output.

The mapping of the pattern into the orientation (fixation) behavior obeys *formally* the rules of a one-to-one correspondence if one takes into account the superposition principle for the pattern-potential relation, and Eqs. (30), (31), for the potential-orientation transformation. Indeed Eq. (31) describes a simple non-linear filter operation upon $U(\psi)$ which is controlled by the parameters b and ζ. Large values of the torque noise (spectral density ζ) determine a quasi-linear transformation from $U(\psi)$ into $p(\psi)$, mapping the complete potential profile with equal weight. Small values of ζ, however, result in a mapping of practically only the minima in $U(\psi)$ into the probability distribution $p(\psi)$. Since the single stripe potential $U_{\text{stripe}}(\psi)$ is non-harmonic (see Fig. 9), the superposition of two or more stripe potentials can easily lead to "symmetry breakings" with regard to the potential minima. The number and the positions of the minima can be considered as order parameters distinguishing different classes of patterns. It is readily seen that small noise powers, mapping only the minima of the potential profile, extract pseudo-invariances from the pattern in the sense that the stationary orientation (fixation) histograms are practically invariant with respect to a class of patterns with the same order parameters.

The formal structure of the theory, as developed so far, suggests the possibility of applying concepts like *phase transitions* to the fly's pattern discrimination behavior. In the two-stripe case, Reichardt (1973), a typical phase transition occurs in the stationary fixation distribution for a value of the parameter $\Delta\psi$ (angular separation of the two stripes) of about 40 degrees. For $\Delta\psi$ values greater than ~ 40 degrees, the previous stable fixation position $\overline{\psi} = 0$ becomes unstable and two new stable positions appear, determined by the corresponding minima of the potential.

Clearly the extension of the experiments and the theory to more dynamical dimensions and pattern parameters than one, may well reveal an even more complex behavior. It is still an open question how one can in this case characterize the induced reaction. Especially, it would be conceivable that the potential description may no longer be valid, because of the non-trivial integrability conditions which, e.g., a two-dimensional field should satisfy.

The orientation theory described so far seems at least to reveal rich classification mechanisms, performing a non-trivial preprocessing of sensory information. The idea that the pattern fixation and discrimination process can be described by a statistical approach and with concepts like phase transition, is appealing, and might potentially lead to interesting developments.

Acknowledgements. We would like to thank Mr. L. Heimburger for his valuable technical assistance in carrying out the experiments and for drawing the figures of this paper.

We acknowledge gratefully various helpful suggestions and criticism of the manuscript by E. Buchner, Dr. J. Coggshall, G. Geiger, Dr. K. G. Götz, Dr. M. Heisenberg, R. Virsik, Ch. Wehrhahn and G. Zimmermann.

Especially we would like to thank Dr. B. Rosser who has contributed with many suggestions also concerning the English text; and Mrs. I. Geiss for typing the manuscript.

Appendix A

Electrophysiological findings, McCann (1972), suggest a lower limit for the delay ε in the induced optomotor response of about 70 msec. Taking values of ε of around 0.1–0.2 [sec] and typical values for the other parameters, the power spectra described by Eq. (16A) were plotted by computer.

Such theoretically derived power spectra agree closely with those obtained experimentally under the conditions of low coupling, $\frac{\Theta}{k} = 4 \cdot 10^{-3}$ and $8 \cdot 10^{-3}$ [sec]. These values were more frequently used and are probably the most physiological ones. Both power spectra have a typical, low-pass shape, and both show only small contributions above 2 Hz. Nevertheless, while this agreement may be made exact, the assumption of zero-delay seems a sufficiently good approximation at *low* coupling.

As expected, Eq. (16a) does not hold for high couplings since the basic conditions for a linearization fail. The speed fluctuations ($\overline{\dot{\psi}^2}$) and the position fluctuations ($\overline{\psi^2}$) are not small and the delay is probably no longer negligible. Not only is the stochastic linearization in Eq. (16a) valid for only one coupling (r, a are, of course, coupling dependent since they depend upon the distributions of ψ and $\dot{\psi}$) but the non-linear dynamics of $D(\psi, \dot{\psi})$ is likely also to play a more direct role. Thus the problem of obtaining the spectrum of $\psi(t)$ for every coupling is an non-linear one, for which the linearization used so far is completely insufficient.

Other approximations may also require reconsideration. It was assumed, for example, that the open loop torque fluctuation represents the noise in the closed loop condition. This may not be so if the stochastic properties (e.g. spectrum, gaussianity) of $N(t)$ depend to some extent upon average receptor stimulation or optomotor activity. This problem is strictly related to the question how the process $N(t)$ is generated. In order to incorporate these additional features, sophistications of our experimental and theoretical work are presently planned.

Appendix B

The autocorrelation function $S_{\psi,\psi}(\tau)$ is obtained by performing the convolution indicated in Eq. (17a) between $S_{T,T}$ and $S_{N,N}$; see Eqs. (17b) and (19). That is

$$S_{\psi,\psi}(\tau) = \frac{1}{\Theta^2} S_{N,N} * S_{T,T} \tag{B.1}$$

$$= \frac{1}{\Theta^2} \int_{-\infty}^{+\infty} \frac{A}{2a \cdot b} \cdot e^{-\frac{b}{2}|t|} \left\{ \cos 2\pi f^* \tau + \frac{b}{4\pi f^*} \cdot \sin 2\pi f^* |\tau| \right\} \cdot e^{-\gamma|\tau - t|} \, dt \,.$$

After integration we obtain $S_{\psi,\psi}(\tau)$

$$= \frac{A}{2b \cdot a \cdot \Theta^2} \left[\frac{e^{-\frac{b}{2}\tau} \left\{ \left(\gamma - \frac{b}{2}\right) \cos 2\pi f^* \tau + 2\pi f^* \sin 2\pi f \tau \right\} - e^{-\gamma\tau} \left(\gamma - \frac{b}{2}\right)}{\left(\frac{b}{2} - \gamma\right)^2 + 4\pi^2 f^{*2}} \right.$$

$$+ \frac{b}{4\pi f^*} \cdot \frac{e^{-\frac{b}{2}\tau} \left\{ \left(\gamma - \frac{b}{2}\right) \sin 2\pi f^* \tau - 2\pi f^* \cos 2\pi f^* \tau \right\} + e^{-\gamma\tau} \cdot 2\pi f^*}{\left(\frac{b}{2} - \gamma\right)^2 + 4\pi^2 f^{*2}}$$

$$+ \frac{e^{-\frac{b}{2}\tau} \left\{ \left(\frac{b}{2} + \gamma\right) \cos 2\pi f^* \tau - 2\pi f^* \sin 2\pi f^* \tau \right\} + e^{-\gamma\tau} \left(\gamma + \frac{b}{2}\right)}{\left(\frac{b}{2} + \gamma\right)^2 + 4\pi^2 f^{*2}} \tag{B.2}$$

$$\left. + \frac{b}{4\pi f^*} \frac{e^{-\frac{b}{2}\tau} \left\{ \left(\frac{b}{2} + \gamma\right) \sin 2\pi f^* \tau + 2\pi f^* \cos 2\pi f^* \tau \right\} + e^{-\gamma\tau} \cdot 2\pi f^*}{\left(\frac{b}{2} + \gamma\right)^2 + 4\pi^2 f^{*2}} \right]$$

valid for $\tau > 0$. The expression for $\tau < 0$ is readily obtained since the autocorrelation is an even function.

Equation (B.2) gives for $\tau = 0$ the much simpler Eq. (20); in fact, it is possible to derive directly the value for σ^2 by integrating Eq. (16b) over the frequency spectrum (and using for example one of the noise response integrals of MacLane, 1947). On the other hand the knowledge of $S_{\psi,\psi}(\tau)$ in principle allows us to characterize completely the statistics of the random process $\psi(t)$. For example the conditional density $P_{\psi(t)}(\psi/\psi_0)$ is a gaussian distribution whose mean is

$$\overline{\{\psi(t)/\psi_0\}} = \frac{S_{\psi,\psi}(t)}{S_{\psi,\psi}(0)} \psi_0 \tag{B.3}$$

and whose variance is

$$\sigma^2_{\psi(t)/\psi_0} = S_{\psi,\psi}(0) - \frac{S^2_{\psi,\psi}(t)}{S_{\psi,\psi}(0)} \,. \tag{B.4}$$

All other conditional probability distributions of the $\psi(t)$ process and its derivatives can be obtained from $S_{\psi,\psi}(t)$ and its derivatives.

Appendix C

It is clear that the main value of the "white" noise assumption is that it enables one to obtain simple analytical solutions, which are at least illustrative of the gross qualitative features of the problem. In fact, while it is easy to write the Fokker-Planck equation when the gaussian random input process is not of the "white" noise type, its exact solution in the presence of some nonlinearity is complicated. In the following we will outline the same problem considered in Section 3.6, but dropping the "white" noise assumption. Complete approximate solutions will be given elsewhere.

We begin with the generalized *Langevin* equation (3)

$$\Theta \ddot{\psi} + k \dot{\psi} + F_1(\psi, \dot{\psi}) = N(t) \tag{C.1}$$

which by Eq. (25) is rewritten as

$$\Theta \ddot{\psi} + (k + r) \dot{\psi} + \frac{\partial}{\partial \psi} U(\psi) = N(t) \tag{C.2}$$

where $N(t)$ is a "non white" random process. Since the value Θ is very small, we can approximate Eq. (C.2) as

$$(k+r)\,\dot{\psi} + \frac{\partial}{\partial \psi} U(\psi) = N(t). \tag{C.3}$$

We assume the random process $N(t)$ to be gaussian and approximable by the one measured under open loop conditions; therefore, its autocorrelation function can be taken to be $S_{N,N}(\tau) = A e^{-\gamma|\tau|}$, implying the following power spectrum

$$\tilde{N}(\omega) = \frac{2A\gamma}{\gamma^2 + \omega^2}, \quad \text{with} \quad \omega = 2\pi f. \tag{C.4}$$

In Eq. (C.3) the process $\psi(t)$ is non-Markovian, because $N(t)$ is of the "non-white" noise type. Moreover, since $U(\psi)$ is not, in general, a harmonic potential, $\psi(t)$ is not even gaussian.

In order to write the Fokker-Planck equation associated with Eqs. (C.3) and (C.4), we may suppose that the process $N(t)$ is obtained by passing "white" noise through a low pass filter. This is equivalent to writing Eqs. (C.3) and (C.4) as

$$\begin{aligned} &\dot{\psi} + \frac{1}{(r+k)} \frac{\partial U}{\partial \psi} = \frac{N(t)}{k+r} \\ &\dot{N} + \gamma N = W(t); \quad S_{W,W}(\tau) = 2A\gamma\delta(\tau). \end{aligned} \tag{C.5}$$

The two differential equations describe the "motion" of our dynamic system in the phase space $[\psi, N]$. $W(t)$ being a stationary gaussian "white" noise process, the trajectory $[\psi(t), N(t)]$ is a two-dimensional Markov process of which $\psi(t)$ is a projection. Equation (C.5) can be rewritten as

$$\begin{aligned} &\dot{\psi} + \frac{\partial U}{\partial \psi} \cdot \frac{1}{(k+r)} = x(t) \\ &\dot{x} + \gamma x = W'(t); \quad S_{W',W'}(\tau) = 2A\gamma \frac{1}{(k+r)^2} \delta(\tau). \end{aligned} \tag{C.6}$$

The average values occuring in the associated Fokker-Planck equation are easily calculated from Eq. (C.6) as

$$\begin{aligned} A_1 &= \lim_{\Delta t \to 0} \frac{\langle \Delta \psi \rangle}{\Delta t} = x - \frac{\partial U}{\partial \psi} \frac{1}{(k+r)} \\ A_2 &= \lim_{\Delta t \to 0} \frac{\langle \Delta x \rangle}{\Delta t} = -\gamma \cdot x \\ B_{11} &= \lim_{\Delta t \to 0} \frac{\langle \Delta \psi^2 \rangle}{\Delta t} = 0 \\ B_{12} &= \lim_{\Delta t \to 0} \frac{\langle \Delta x \Delta \psi \rangle}{\Delta t} = 0 \\ B_{22} &= \lim_{\Delta t \to 0} \frac{\langle \Delta x^2 \rangle}{\Delta t} = 2A\gamma \frac{1}{(k+r)^2}. \end{aligned} \tag{C.7}$$

The Fokker-Planck equation corresponding to Eq. (C.6) is readily obtained as

$$\frac{\partial}{\partial t} p = \frac{\partial}{\partial \psi}\left(x - \frac{\partial U(\psi)}{\partial \psi} \cdot \frac{1}{(k+r)}\right) \cdot p + \frac{\partial}{\partial x}(\gamma \cdot x \cdot p) + \frac{A\gamma}{(k+r)^2} \frac{\partial^2}{\partial x^2} p. \tag{C.8}$$

Since $-\dfrac{\partial U}{\partial \psi}$ is a piecewise linear function, $U(\psi)$ can be well approximated around every stable equilibrium point (like ψ_0 in Fig. 13) by

$$U(\psi)_{\text{near } \psi_0} = \frac{1}{2} \alpha \psi^2 \tag{C.9}$$

and, around the unstable equilibrium points (like ψ_b), by

$$U(\psi)_{\text{near } \psi_b} = E - \frac{1}{2}(\psi - \psi_b)^2 \alpha'. \tag{C.10}$$

Therefore, defining $\dfrac{\alpha}{k+r} = l$; $\dfrac{\alpha'}{k+r} = l'$; $\dfrac{A\gamma}{(k+r)^2} = d$ we obtain from Eq. (C.8)

$$\frac{\partial p}{\partial t} = -\frac{\partial}{\partial \psi}(x - l\psi)\, p + \frac{\partial}{\partial x}(\gamma x p) + d \frac{\partial^2 p}{\partial x^2} \tag{C.11}$$

around $\psi_0 = 0$, and

$$\frac{\partial p}{\partial t} = -\frac{\partial}{\partial \psi'}(x + l'\psi')\, p + \frac{\partial}{\partial x}(\gamma x p) + d \frac{\partial^2 p}{\partial x^2} \tag{C.12}$$

around $\psi_b (\psi' = \psi - \psi_b)$.

To solve these equations we diagonalize them with the transformation

$$\begin{aligned} &z_1 = x \\ &z_2 = x + (\gamma - l)\,\psi \quad \text{or} \quad z_2' = x + (\gamma + l')\,\psi'. \end{aligned} \tag{C.13}$$

Substituting in the previous equations we get

$$\frac{\partial p}{\partial t} = \frac{\partial}{\partial z_1}(\gamma z_1 p) + \frac{\partial}{\partial z_2}(l z_2 p) + d\left[\frac{\partial}{\partial z_1} + \frac{\partial}{\partial z_2}\right]^2 \cdot p \tag{C.14}$$

near ψ_0 and

$$\frac{\partial p}{\partial t} = \frac{\partial}{\partial z_1}(\gamma z_1 p) - \frac{\partial}{\partial z_2'}(l' z_2' p) + d\left[\frac{\partial}{\partial z_1} + \frac{\partial}{\partial z_2'}\right]^2 \cdot p \tag{C.15}$$

near ψ_b.

We treat the problem as a stationary one. Taking the limit for $t \to \infty$ of the solutions of Eqs. (C.14) and (C.13) we get the stable distributions

$$p(\psi, x) = C e^{-\frac{l+\gamma}{d}\left[\frac{l(l+\gamma)}{2}\psi^2 + \frac{1}{2}x^2 - l\psi x\right]} \tag{C.16}$$

near $\psi_0 = 0$ and

$$p(\psi', x) = C' e^{-\frac{\gamma - l'}{d}\left[\frac{-l'(\gamma - l')}{2}\psi'^2 + \frac{1}{2}x^2 + l'\psi' x\right]} \tag{C.17}$$

near ψ_b. Around ψ_0 we find

$$p(\psi) = C \sqrt{\frac{2\pi d}{l+\gamma}}\, e^{-\frac{(l+\gamma)\gamma \cdot l}{2d}\psi^2} \tag{C.18}$$

which is a gaussian distribution with

$$\sigma^2 = \frac{A}{[(k+r)\gamma + \alpha]\,\alpha}. \tag{C.19}$$

It should be mentioned that Eq. (20) reduces, in the limit of $\Theta \to 0$, to Eq. (C.19). Around ψ_b we find

$$p(\psi') = C' \sqrt{\frac{2\pi d}{\Delta}}\, e^{+\frac{\Delta\gamma l'}{2d}\psi'^2} \tag{C.20}$$

where $\Delta = \gamma - l' = \gamma - \dfrac{\alpha'}{k+r}$.

It is, of course, required that $\Delta > 0$.

It is also possible to find the probability distribution around ψ_b under quasi stationary assumptions, such as

$$p(\psi', x) = C'' e^{-\frac{\Delta}{2d}\left[-\Delta l'\psi'^2 + x^2 + 2l'\psi' x\right]} \cdot \sqrt{\frac{l'}{2\pi d}} \int_{-\infty}^{+\zeta} d\zeta\, e^{-\frac{l'}{2d}\zeta^2}. \tag{C.21}$$

where $\zeta = x - m\psi'$ and m is chosen as $m = \gamma - l'$ under the condition $m > 0$.

A tentative solution for the probability of barrier crossing at ψ_b, can be outlined as follows: We rewrite Eq. (C.8)

$$\frac{\partial p}{\partial t} = \left[\frac{\partial}{\partial x} - \frac{1}{\gamma}\frac{\partial}{\partial \psi}\right]\left[\gamma x p + d\frac{\partial}{\partial x}p + \frac{d}{\gamma}\frac{\partial}{\partial \psi}p\right] - \frac{\partial}{\partial \psi}\left[-\frac{\partial U}{\partial \psi}\frac{1}{(k+r)} - \frac{d}{\gamma^2}\frac{\partial p}{\partial \psi}\right]. \tag{C.22}$$

We integrate first along $\psi + \frac{x}{\gamma} = \psi_0$; then assume the approximation $p(\psi, x, t) \approx \sigma(\psi, t)\, e^{-x^2 \cdot \text{const}}$ and finally that in the domain where the main contribution to the integral arises, the variation of ψ is small. Then it follows

$$\frac{\partial \sigma(\psi, t)}{\partial t} = -\frac{\partial}{\partial \psi_0}\left[-\frac{1}{k+r}\frac{\partial U}{\partial \psi}\sigma(\psi_0) - \frac{d}{\gamma^2}\frac{\partial \sigma}{\partial \psi_0}\right]. \tag{C.23}$$

A stationary diffusion current j is defined by

$$j = \frac{\left[\sigma e^{+\frac{U}{(k+r)}\cdot\frac{\gamma^2}{d}}\right]_{\psi_0}^{\psi_0}}{\int_{\psi_0}^{\psi_b} e^{+\frac{\gamma^2}{d}\frac{U}{(k+r)}} d\psi} \cdot \frac{d}{\gamma^2}. \tag{C.24}$$

Quasistationary conditions imply that

$$j = \frac{d}{\gamma^2}\sigma(\psi_0)\frac{1}{\int_{\psi_0}^{\psi_b} e^{+\frac{\gamma^2}{d(k+r)}U(\psi)} d\psi}, \tag{C.25}$$

where

$$\sigma(\psi_0) = C\sqrt{\frac{2\pi d}{l+\gamma}}\, e^{-\frac{(l+\gamma)l\gamma}{2d}\psi^2}\Big|_{\psi=\psi_0=0} \cdot e^{\frac{\gamma^2}{d(k+r)}U(\psi_0)}.$$

From Eq. (C.18) we obtain the normalization factor C

$$C = \frac{\gamma + l}{2\pi d}\sqrt{l\gamma} \tag{C.26}$$

and, therefore, the probability per unit time for the stripe to escape across ψ_b is

$$p_b = \frac{1}{2\pi}\frac{1}{(k+r)}\sqrt{1 + \frac{\alpha}{(k+r)\gamma}}\sqrt{\alpha \cdot \alpha'}\, e^{-\frac{\gamma(k+r)}{A}E}. \tag{C.27}$$

One can easily prove that Eq. (C.27), in the limit of "white noise" ($\gamma \to \infty$, $A\alpha\gamma$) approaches the form of Eq. (41). In this connection we recall that the limit at which the low pass noise spectrum changes into "white noise" is given by

$$\left(\frac{2A\gamma}{\gamma^2 + 4\pi^2 f^2}\right)_{\lim \gamma \to \infty,\, A = c\gamma} \to 2c\,[\text{spectral density}]. \tag{C.28}$$

Then Eq. (C.27) under the same limiting conditions [using (C.28)], becomes

$$(p_b)_{\lim \gamma \to 0,\, A = c\gamma} = \frac{1}{2\pi(k+r)}\sqrt{\alpha \cdot \alpha'}\, e^{-\frac{k+r}{c}E} \tag{C.27}$$

which is equal to Eq. (41).

A numerical evaluation of Eq. (C.27) in the case of the potential profile generated by the single stripe (see Fig. 9) is given in the text.

In conclusion, the usefulness of this approach to the non-white noise case is mainly in giving the conditions under which it is approximated by the white noise one. From Eqs. (C.18), (C.20), (C.27), it turns out that the white noise stationary solutions of Section 3.6 are a good approximation (with $c = A/\gamma$) if the condition $\gamma(k+r) \gg \alpha$ holds, where α here represents the maximum slope of the potential profile.

Appendix D

Following Kramers' (1940) approach to the diffusion model of chemical reactions, we seek a solution of Eq. (34) in the form

$$p(\psi', w) = C e^{-\frac{Eb}{\theta\zeta}} R(\psi', w)\, e^{-(w^2 - a'\psi'^2)\cdot\frac{b}{2\zeta}} \tag{D.1}$$

which, substituted in Eq. (35), gives

$$0 = -a'\psi'\frac{\partial R}{\partial w} - p\frac{\partial R}{\partial \psi'} - bp\frac{\partial R}{\partial w} + \zeta\frac{\partial^2 R}{\partial w^2}. \tag{D.2}$$

Of course, $R = \text{const}$ is equivalent to thermal equilibrium, i.e. there is then no net probability flow from ψ_0 to ψ_b. It is required however, that the probability distribution (D.1) will approach the equilibrium around $\psi = \psi_0$, falling off to zero far to the right of ψ_b where, because of the quasi-stationary conditions, the probability of the stripe positioning must be negligible. These conditions are expressed formally by

$$\begin{aligned} &R(\psi', w) \to 1 \quad \text{for} \quad \psi' \cong -\psi_b \\ &R(\psi', w) \to 0 \quad \text{for} \quad \psi' \gg 0. \end{aligned} \tag{D.3}$$

Assuming

$$R = R(\varrho) \qquad \varrho = w - \mu\psi' \tag{D.4}$$

and substituting in Eq. (D.2), we get

$$0 = [(\mu - b)w - a'\psi']\frac{dR}{d\varrho} + \zeta\frac{d^2 R}{d\varrho^2} \tag{D.5}$$

which, with the condition

$$\mu = \frac{b}{2} + \sqrt{\frac{b^2}{4} + a'}, \tag{D.6}$$

has the solution

$$R(\psi', w) = \sqrt{\frac{\mu - b}{2\pi\zeta}}\int_{-\infty}^{\varrho} e^{-(\mu-b)\frac{\varrho^2}{2\zeta}} d\varrho. \tag{D.7}$$

Clearly R satisfies the boundary conditions (D.3), since

$$\begin{aligned} &R \to 1 \quad \text{for} \quad \varrho \to \infty \\ &R \to 0 \quad \text{for} \quad \varrho \to -\infty. \end{aligned} \tag{D.8}$$

Equations (D.1) and (D.7) finally lead to Eq. (37).

The probability flow across the barrier is given by Eq. (38) which is

$$j_b = \int_{-\infty}^{+\infty} p_b(\psi' = 0, w)\, w\, dw.$$

Equation (38) can be rewritten as

$$j_b = C\sqrt{\frac{(\mu - b)}{2\pi\zeta}}\, e^{-\frac{Eb}{\zeta\theta}} \int_{-\infty}^{+\infty} dw \cdot w \cdot e^{-w^2\frac{b}{2\zeta}} \int_{-\infty}^{w} e^{-\frac{(\mu-b)}{2\zeta}\varrho^2} d\varrho \tag{D.9}$$

which, integrated by parts, gives

$$j_b = C\sqrt{\frac{(\mu-b)}{2\pi\zeta}}\, e^{-\frac{Eb}{\zeta\Theta}}\left\{\left[-e^{-w^2\frac{b}{2\zeta}}\frac{\zeta}{b}\int_{-\infty}^{w} e^{-\frac{(\mu-b)}{2\zeta}e^2}\,d\varrho\right]_{-\infty}^{+\infty} + \int_{-\infty}^{+\infty}\frac{\zeta}{b}e^{-w^2\frac{b}{2\zeta}}e^{-\frac{(\mu-b)w^2}{2\zeta}}\,dw\right\}$$

$$= C\sqrt{\frac{(\mu-b)}{2\pi\zeta}}\, e^{-\frac{Eb}{\zeta\Theta}}\cdot\frac{\zeta}{b}\int_{-\infty}^{+\infty} e^{-\frac{\mu}{2\zeta}w^2}\,dw$$

$$= C\sqrt{\frac{(\mu-b)}{\mu}}\cdot\frac{\zeta}{b}\cdot e^{-\frac{Eb}{\Theta\zeta}}.$$

The constant C is then normalized using Eq. (36) through

$$1 = \int_{-\pi}^{+\pi}\int_{-\infty}^{+\infty} C e^{-(w^2+a\psi^2)\frac{b}{2\zeta}}\,dw\,d\psi\,; \qquad \text{(D.11)}$$

we get $C = \dfrac{b\sqrt{a}}{2\zeta\pi}$.

Equation (40) becomes in the limiting case of $\dfrac{b^2}{4} \gg a'$

$$p_b = \frac{\sqrt{a}}{2\pi\sqrt{a'}}\left[\sqrt{1+\frac{4a'}{b^2}}-1\right]\cdot\frac{b}{2}\cdot e^{-\frac{Eb}{\Theta\cdot\zeta}}$$

$$\cong \frac{\sqrt{a}}{2\pi\sqrt{a'}}\cdot\frac{b}{2}\cdot e^{-\frac{Eb}{\Theta\zeta}}\left[1+\frac{2a'}{b^2}-1\right]$$

$$= \sqrt{a\cdot a'}\,\frac{1}{2\pi b}\cdot e^{-\frac{Eb}{\Theta\cdot\zeta}}.$$

References*

Fermi, G., Reichardt, W.: Optomotorische Reaktionen der Fliege *Musca domestica*. Kybernetik **2**, 15 (1963).

Götz, K. G.: Optomotorische Untersuchung des visuellen Systems einiger Augenmutanten der Fruchtfliege *Drosophila*. Kybernetik **2**, 77 (1964).

Kasakov, I. E.: Automatic and remote control. Proc. I. Int. Congr. IFAC, Moscow 1960. Ed. Coales, J. F. London: Butterworth 1961.

Kramers, H. A.: Brownian motion in a field of force. Physica VI, **4**, 284 (1940).

MacLane, G. R.: In: Theory of servomechanisms. Ed. James, H. M., Nichols, N. B., Phillips, R. S. 369: McGraw Hill 1947.

McCann, G. D.: The fundamental mechanism of motion detection in the insect visual system. Kybernetik **12**, 64 (1973).

Oyster, C. W.: The analysis of image motion by the rabbit retina. J. Physiol. **199**, 613 (1968).

Poggio, T.: Outline of a model of spontaneous fixation by the visual system of flies. In: Atti del Congresso (1972) di Cibernetica (GRC-CNR) (in press).

Reichardt, W.: Autocorrelation, a principle for evaluation of sensory information by the central nervous system. In: Principles of Sensory Communications. Ed. Rosenblith, W. A. 303: John Wiley 1961.

Reichardt, W., Wenking, H.: Optical detection and fixation of objects by fixed flying flies. Naturwissenschaften **56**, 424 (1969).

Reichardt, W.: The insect eye as a model for analysis of uptake, transduction and processing of optical data in the nervous system. 34. Physikertagung, Plenarvorträge Teubner Stuttgart (1969a).

Reichardt, W.: Movement perception in insects. Rendiconti della Scuola Internazionale di Fisica "Enrico Fermi" Corso XLIII, 465—493. New York, London: Academic Press 1969b.

Reichardt, W.: The insect eye as a model for analysis of uptake, transduction, and processing of optical data in the nervous system. In: The Neurosciences, Second Study Program, Ed. Schmitt, F. O. New York: The Rockefeller University Press 1970.

Reichardt, W.: Visual detection and fixation of objects by fixed flying flies. In: Zeichenerkennung durch biologische und technische Systeme. Berlin-Heidelberg-New York: Springer 1971a.

Reichardt, W.: The insect eye as a model for processing of optical data in the nervous system. Proceedings Vol. V. Cells, Organs. First European Biophysics Congress (1971b).

Reichardt, W.: Musterinduzierte Flugorientierung der Fliege *Musca domestica*. Naturwissenschaften **60**, 122 (1973).

Richards, W., Kaufman, L.: Center-of-gravity. Tendencies for fixations and flow patterns. Perception & Psychophysics **5**, 2 (1969).

Vasudevan, R., Pathak, A. V., Smith, J. D.: A stochastic model for eye movements during fixation on a stationary target. Kybernetik **11**, 24 (1972).

Virsik, R.: In preparation.

Wax, N.: Noise and stochastic processes. New York: Dover Inc. 1954.

Wehrhahn, C., Reichardt, W.: Visual orientation of the fly *Musca domestica* to a horizontal stripe. Naturwissenschaften **60**, 203 (1973).

Prof. Dr. W. Reichardt
Max-Planck-Institut
für biolog. Kybernetik
D-7400 Tübingen, Spemannstr. 38
Bundesrepublik Deutschland

* In this paper we have cited only some of the work related to our results. A discussion of the experimental results obtained by many other authors seems to be too early at the present state of our investigation.